

An analytical model for secondary phase dissolution kinetics

Qiang Zuo · Feng Liu · Lei Wang · Chang Feng Chen ·
Zhong Hua Zhang

Received: 1 August 2013 / Accepted: 30 December 2013 / Published online: 22 January 2014
© Springer Science+Business Media New York 2014

Abstract An analytical model for dissolution kinetics of secondary phase particles upon isothermal annealing has been proposed. Considering the interactions of solute diffusion fields in front of the secondary phase/matrix interface upon dissolution, a Johnson–Mehl–Avrami type equation, subjected to necessary modification, was derived, in combination with a classic dissolution model for single-particle system. Compared with the semiempirical dissolution models, which are used to fit the experimental results and phase-field method simulation, the current model follows an analogous form, but with the time-dependent kinetic parameters. Distinct from the model fitting work published recently, the current model is derived from the diffusion-controlled transformation theory, while the modeling quality is guaranteed by the physically realistic model parameters. On this basis, the current model calculation leads to a clear relationship between the secondary phase volume fraction and the time. Accordingly, model predictions for isothermal θ' dissolution in Al–3.0wt%–Cu alloy and silicon dissolution in Al–0.8wt%–Si alloy were performed; good agreement with the published experimental data has been achieved.

List of symbols

C_m	Initial solute concentration in the matrix
C_α	Solute concentration at the interface
C_β	Solute concentration in the secondary phase
D	Diffusion coefficient of solute atoms
D_0	Preexponential factor for diffusion
f	Volume fraction of the secondary phase
f_0	Initial volume fraction of the secondary phase
f_{eq}	Equilibrium volume fraction of the secondary phase
f_t	Transformed fraction (transformation degree)
k	Dimensionless parameter related to solute concentrations, C_β , C_α , and C_m
K_0	Rate constant
m	Modified proportional factor
n	Transformed exponent
Q	Activation energy for dissolution
Q_D	Activation energy for diffusion
r_d	Decrement of the dissolving particle radius
R	Radius of the dissolving particle
R_0	Initial radius of the dissolving particle
t_e	The total transformation time needed for dissolution
V_e	Extended transformed volume of the secondary phase
x_e	Extended transformed fraction

Q. Zuo · F. Liu (✉) · L. Wang
State Key Laboratory of Solidification Processing, Northwestern
Polytechnical University, Xi'an 710072, Shaanxi, People's
Republic of China
e-mail: liufeng@nwpu.edu.cn

C. F. Chen
Department of Materials Science and Engineering, China
University of Petroleum, Beijing 102249, People's Republic of
China

Z. H. Zhang
Baoshan Iron & Steel Co., Ltd., Shanghai 201900, People's
Republic of China

Introduction

Secondary phases in alloys are of great impact on physical and chemical properties of materials; so that precipitation and dissolution of such phases have been studied extensively [1–3]. Upon material processing, the secondary phase would precipitate from alloys during isothermal aging or continuous cooling process, whereas, such

precipitates could be removed by homogenization, where the alloy is heated up to a temperature of single-phase region of phase diagram to dissolve the secondary phase and achieve a homogenized microstructure. Using analytical, experimental and numerical methods, lots of studies have been carried out for secondary phase precipitation in the past decades [4–13]. As compared to flourishing studies of precipitation from supersaturated solid solution, however, the corresponding works on dissolution of the secondary phase are relatively few, most of which are focused on describing qualitatively the microstructure evolution [14–18].

Analogous to the precipitation process, dissolution of the secondary phase during homogenization is controlled by solute diffusion. Accordingly, Thomas and Whelan [19] proposed a simple model considering that dissolution is approximately a reversal of precipitation. Based on a linear concentration field approximation, however, Aaron [20] investigated the one-dimensional (1D) dissolution process and found that dissolution cannot be regarded simply as a reversal of precipitation, but involving a series of complicated mathematical description. Shortly, by solving the diffusion equations under assumptions of stationary interface and local equilibrium at the interface, Whelan [21] proposed a kinetic model for three-dimensional (3D) dissolution, which, subsequently, was used widely. Thereafter, Aaron et al. [22] revealed that no exact analytical solution holds for secondary phase dissolution in 3D, and Whelan's model offers the most accurate solution. Later on, effect of curvature on dissolution kinetics was considered [23–25], while Aaron and Kotler [24] concluded that, for most alloy systems, such effect can be negligible, unless the difference between solute concentration at the particle/matrix interface and that in the matrix far from the interface is extremely small. This was confirmed by subsequent investigations by Nojiri and Enomoto [25]. Also, the same authors, in another paper [26], proposed a numerical solution for dissolution of spherical precipitates in an infinitely large matrix. All these models were limited to dissolution of single-particle system, where the interactions of multi-particle dissolution were not considered.

It was demonstrated by Brown [27] that the interactions of multi-particle dissolution would slow down the transformation rate. So the above models [19–26] for single-particle dissolution could not describe accurately the real dissolution process. In order to deal with the multi-particle dissolution, many numerical models have been developed. For examples, using a finite difference technique, Tanzilli and Heckel [28, 29] developed a numerical model for dissolution kinetics, which indicated that the composition at the midpoint of two dissolving particles changes early in the process and this overlap of adjacent diffusion fields slows down the dissolution process. In another paper Baty

et al. [30], studied the dissolution kinetics of CuAl_2 in Al–Cu alloy and presented a method to predict the variation of the particle size distribution during the annealing process. Moreover, Tundal and Ryum [31] investigated that the dissolution process in binary alloys during isothermal annealing by a numerical method. And based on a mathematical method which is applicable to dissolution of multi-component phases in ternary media, Vermolen et al. [32] studied the dissolution kinetics of Mg_2Si in Al–Mg–Si alloys.

Recently, phase-field method (PFM) and computational tools were applied to deal with the dissolution process [33–40]. Using PFM, Chen and Wang [36] simulated successfully the dissolution process of primary particles in an Al alloy during isothermal homogenization. Utilizing a three-dimensional quantitative PFM, Wang et al. [37] proposed a model for dissolution kinetics considering the effect of initial particle size distribution in Ni–Al alloys. Moreover, Ghosh [38] simulated the dissolution kinetics of Ag-layer in liquid solder using computational thermodynamics (Thermo-Calc) and kinetics (DICTRA) tools, in conjunction with the assessed thermodynamical and mobility data. With input from CHLPHAD and DICTRA databases, dissolution of a globular α precipitate in Ti–Al–V was simulated quantitatively in 2D using PFM, and the results agree well with DICTRA simulations [39]. Applying JMatPro software, dissolution of primary particles in Al alloys was simulated by Kovacevic and Sarler [40]. However, such numerical methods require considerable computational effort and thus become too inconvenient for direct application.

As mentioned above, the early analytical models cannot describe the dissolution process accurately, while the numerical methods are inconvenient for direct application. Therefore, several semiempirical models [41–44] have been proposed recently to overcome such negative features of analytic and numerical methods. By experimentally dissolving γ' phase in Ni-based superalloy, Cormier et al. [41] got an asymptotic exponential equation, which can be used to describe the evolution of γ' fraction with time. Shortly, Giraud et al. [42] concluded that the exponential equation proposed by Cormier was in reality deduced from the Johnson–Mehl–Avrami (JMA) type function, which offers the best description of heterogeneous transformation. Analogous results were obtained by Fukumoto et al. [43] on studying the δ -ferrite dissolution behavior in an austenitic stainless steel. Moreover, by fitting the numerical results due to PFM, Wang et al. [37] found that the volume fraction of secondary phase decayed exponentially with time, and obtained a JMA-like equation. Based on Wang's work, Ferro [44] proposed a semiempirical model where an impingement factor was introduced, and such model was successfully applied to isothermal dissolution of σ phase in

a duplex stainless steel. However, these models, following a simple mathematical form, are not derived from the diffusion kinetics during dissolution, so that the kinetic parameters used in these models could be obtained only by model fittings to the experimental data. Such semiempirical models could not reflect really the transformation kinetics upon dissolution.

In conclusion, the following problems still exist for modeling the real multi-particle dissolution process, so far. (1) No proper analytical method is available to deal with the interaction of adjacent particles during dissolution. (2) Solution to diffusion equations for dissolution is still in numerical form and inconvenient for direct application. In order to solve the above problems, it is herein aimed to develop an analytical model for the secondary phase dissolution kinetics, in combination with the JMA theory [6, 7] and the classic dissolution equation [21].

Model derivation

To analyze the dissolution kinetics, a concept of transformation degree (transformed fraction), f_t , which is defined by Mittemeijer [45] should be introduced.

$$f_t \equiv (p - p_0)/(p_1 - p_0) \quad 0 \leq f_t \leq 1 \quad (1)$$

where p is the physical property measured during the course of transformation and p_0 and p_1 correspond to the values of p at the start and the end of the transformation, respectively. Upon dissolution, f_t can be expressed as,

$$f_t = \frac{f - f_0}{f_{\text{eq}} - f_0} \quad (2)$$

where f represents the volume fraction of the secondary phase during dissolution, f_0 and f_{eq} correspond to the initial and the equilibrium volume fraction of the secondary phase, respectively. As for heterogeneous transformations, a JMA-type equation is generally applied to describe the transformed fraction at a given time considering the hard impingement of adjacent particles in multi-particle system [45, 46]. However, for diffusion-controlled transformations, such as precipitation and dissolution, the impingement of solute diffusion fields in front of the secondary phase particle/matrix interface, i.e., soft impingement will occur instead of hard impingement [27, 37, 44]. By modifying some kinetic parameters, the JMA theory is used as a good approximation for such diffusion-controlled transformations [6, 7]. Moreover, semiempirical models [41–44] for dissolution are concluded to be derived from the JMA theory, and their predictions agree well with correspondingly experimental results. So, in the current work, JMA theory is introduced to deal with the dissolution transformation in multi-particle systems.

The classic JMA equation is expressed as [46],

$$f_t = 1 - \exp(-x_e) \quad (3)$$

where x_e represents the extended transformed fraction, which is defined as the volume fraction transformed by neglecting the interactions of adjacent particles. Upon dissolution of the secondary phase, it can be expressed as, $x_e = V_e/V_0$ where V_e represents the extended transformed volume of the secondary phase, i.e., the volume transformed with neglecting the interactions of adjacent particles and V_0 represents the initial volume of the secondary phase.

If the empirical expression, $x_e = (Kt)^n$ is applied, then combining Eqs. (2) and (3), the expression of semiempirical dissolution model [37, 41–44] follows,

$$f = f_{\text{eq}} + (f_0 - f_{\text{eq}}) \exp(-K^n \cdot t^n) \quad (4)$$

By fitting Eq. (4) to the experimental results, proper values of parameters, n and K , can be determined to describe the real dissolution behavior [37, 41–44]. However, such semiempirical equation is derived from simply applying the classic JMA theory for crystal growth [37, 41–44] and does not consider the real solute diffusion process during dissolution.

Therefore, the current model calculation is proposed by studying the real diffusion-controlled dissolution process, to guarantee a physically sounded kinetic analysis. Based on the analysis of solute diffusion process during dissolution, the extended transformed volume, V_e , is described first, and then the interactions of multi-particle dissolution are considered, and finally, a concise and simple analytical model for dissolution kinetics is obtained.

A description for extended transformed volume

Without considering the interactions of adjacent particles, the extended volume of the secondary phase during single-particle dissolution is calculated, and then the sum of the extended volume of each particle gives V_e . For simplicity, it is herein assumed that the initial sizes of the secondary phase particles hold all the same. On this basis, an analysis for single secondary phase particle dissolution must be performed firstly.

As a diffusion-controlled process, dissolution is characterized by a solute concentration profile in front of the secondary phase/matrix interface, as shown in Fig. 1. The radius of the dissolving particle, i.e., the position of the interface front, is denoted as R , while R_0 represents the initial radius of the dissolving particle. The solute concentration of the secondary phase, C_β , is taken as a constant independent of the position, r , and time, t . C_α and C_m represent the solute concentration at the interface and the far field in the matrix, respectively. Upon single-particle

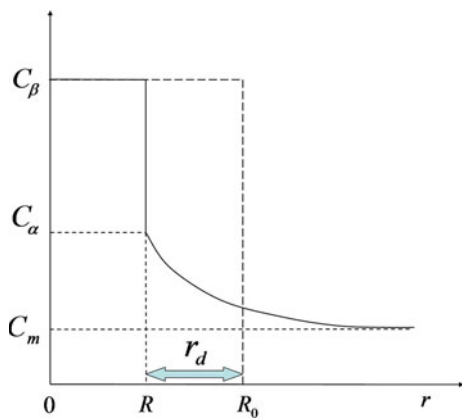


Fig. 1 A schematic diagram of the solute concentration profile in the vicinity of the secondary phase during dissolution. C_β is the solute concentration of the secondary phase; C_α and C_m are the concentration in the matrix at the interface and the far field, respectively. The decrement of the particle radius is denoted as r_d

dissolution, solute diffusion in the matrix can be described by the classical diffusion equation,

$$\frac{\partial C(r,t)}{\partial t} = D \cdot \nabla^2 C(r,t) \tag{5}$$

where the concentration $C(r,t)$ changes as function of r and t . The diffusion coefficient D is assumed to hold constant during the isothermal transformation. Upon dissolution, the solute conservation at the interface leads to another equation, as,

$$(C_\beta - C_\alpha) \cdot \frac{dR}{dt} = D \frac{\partial C}{\partial r} \Big|_{r=R}. \tag{6}$$

Actually, an accurately analytical solution to the above governing equations cannot be obtained; several approximately analytical solutions under various assumptions have been proposed.

Classical model for single-particle dissolution

Among the approximately analytical solutions, the one developed by Whelan under the assumption of stationary interface is generally acknowledged to be the best one [21, 22, 37], which can be expressed as,

$$\frac{dR}{dt} = -\frac{kD}{2R} - \frac{k}{2} \sqrt{\frac{D}{\pi t}} \tag{7}$$

where,

$$k = \frac{2(C_\alpha - C_m)}{C_\beta - C_\alpha} \tag{8}$$

From Ref. [21], the term in R^{-1} on the right-hand side of Eq. (7) arises from the steady-state part, and the term in $t^{-1/2}$ arises from the transient part, of the diffusion field.

Clearly, an analytical solution of such a differential equation cannot be obtained [21, 22], however, by neglecting the transient part or assuming the steady-state part as constant, a concise $R-t$ relationship can be deduced. Of course, the solution due to these rough approximations deviates significantly from the accurate solution, so that it is timely to provide an analytical description for single-particle dissolution, using an approximation considering both the steady-state and transient parts of the diffusion field.

Analytical expression for single-particle dissolution

As shown in Fig. 1, upon dissolution of a single particle, the decrement of the particle radius can be denoted as r_d , which characterizes the transformed amount of the secondary phase, and can be expressed as,

$$r_d = R_0 - R \tag{9}$$

with $r_d = 0$ at $t = 0$; $r_d = R_0$, at $t = t_e$, with t_e as the time when dissolution completes. Then Eq. (7) can be rewritten as,

$$\frac{dr_d}{dt} = \frac{kD}{2(R_0 - r_d)} + \frac{k}{2} \sqrt{\frac{D}{\pi t}} \tag{10}$$

Following the basic philosophy of Ref. [21], the transformed velocity, dr_d/dt , is contributed by two parts: the term in $(R_0 - r_d)^{-1}$ for the steady-state part and the term in $t^{-1/2}$ for the transient part. Suppose r_d as contributed from the two parts as well. If the contributions of steady-state part and transient part are denoted as r_1 and r_2 , and once the dissolution completes, i.e., $t = t_e$, the total contributions of steady-state part and transient part are denoted as R_1 and R_2 , respectively, the following relationship can be obtained,

$$\begin{cases} r_1 + r_2 = r_d \\ R_1 + R_2 = R_0 \end{cases} \tag{11}$$

with $r_1 = r_2 = 0$ at $t = 0$; $r_1 = R_1$, $r_2 = R_2$ at $t = t_e$.

The transformation mechanism due to the steady-state part can be described as,

$$\frac{dy}{dt} = \frac{kD}{2(Y - y)} \tag{12}$$

where y represents the physical property measured during the course of transformation and Y corresponds to the values of y at the end of the transformation. Therefore, in this case the steady-state part can be expressed approximately as,

$$\frac{dr_1}{dt} = \frac{kD}{2(R_1 - r_1)} \tag{13}$$

A combination of Eq. (13) with the boundary conditions, i.e., when $t = 0$, $r_1 = 0$, leads to,

$$r_1 = R_1 - \sqrt{R_1^2 - kDt} \quad (14)$$

Analogously, the transient part can be expressed as,

$$\frac{dr_2}{dt} = \frac{k}{2\sqrt{\pi}} \cdot \sqrt{\frac{D}{t}} \quad (15)$$

A combination of Eq. (15) with the boundary conditions, i.e., when $t = 0$, $r_2 = 0$, leads to,

$$r_2 = \frac{k}{\sqrt{\pi}} \cdot \sqrt{Dt} \quad (16)$$

Substituting Eqs. (14) and (16) into Eq. (11), the decrement of the particle radius, r_d , can be obtained,

$$r_d = R_1 - \sqrt{R_1^2 - kDt} + \frac{k}{\sqrt{\pi}} \cdot \sqrt{Dt} \quad (17)$$

It is known that $t = t_e$ corresponds to $r_1 = R_1$ and $r_2 = R_2$, i.e.,

$$\begin{cases} R_1 = R_1 - \sqrt{R_1^2 - kDt_e} \\ R_2 = \frac{k}{\sqrt{\pi}} \cdot \sqrt{Dt_e} \end{cases} \quad (18)$$

In combination with Eq. (11), the total time needed for dissolution, t_e , can be obtained,

$$t_e = \frac{R_0^2}{kD \left(1 + \sqrt{\frac{k}{\pi}}\right)^2} \quad (19)$$

Then R_1 can be expressed as,

$$R_1 = \frac{1}{\left(1 + \sqrt{\frac{k}{\pi}}\right)} \cdot R_0 \quad (20)$$

Given the parameter R_1 in Eq. (17) experimentally, the decrement of the particle radius, r_d , can then be expressed as a concise function of time. Besides, a clear relationship between the radius of the secondary phase, R , and the time can be obtained,

$$R = \sqrt{\frac{k}{\pi}} \cdot \left(R_1 - \sqrt{kDt}\right) + \sqrt{R_1^2 - kDt} \quad (21)$$

Equation (21) is not mathematically an exact solution to Whelan's equation (Eq. 7), but an approximate one. Comparison of the current solution (Eq. 21) with the exact solution due to Whelan is shown in Fig. 2, which indicates that the current analytical solution gives a good approximation of the exact solution to Eq. (7). Fig. 2a illustrates θ' dissolution in Al–Cu alloy at 370 °C, such a low solution temperature means the thermodynamic driving force for dissolution is small, while Fig. 2b illustrates the dissolution occurred at 540 °C, which means that the corresponding driving force is large. It can be seen good agreements with the numerical calculation are obtained in both of the above cases. Moreover, each term in the right-hand side of Eq. (21) is plotted in Fig. 2, and the second term is found to be the dominant role. Values for the calculation parameters used are chosen from θ' dissolution in Al–Cu alloy [15, 30], as listed in Table 1. Also, the current solution owns a clear and simple form and is convenient for direct application.

Then, the extended transformed volume, V_e , can be expressed as,

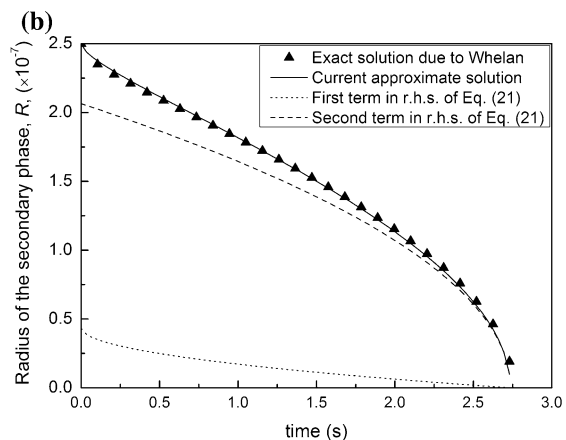
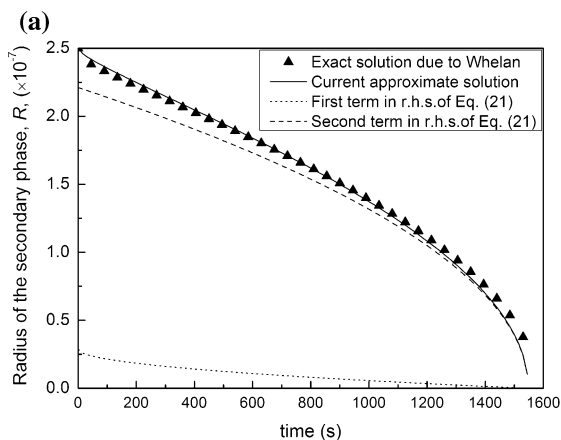


Fig. 2 Comparison of the current approximate solution (Eq. 21) with the exact solution due to Whelan (Eq. 7). Each term in the right-hand side of Eq. (21) is plotted as well. **a** The transformation occurs at 370 °C, which corresponds to the small thermodynamic driving force

for dissolution; **b** the dissolution occurs at 540 °C, which corresponds to the large driving force. Values for the calculation parameters used are chosen from θ' dissolution in Al–Cu alloy [15, 30]

Table 1 Values of parameters used for numerical and analytical calculations

T (°C)	R_0 (μm)	C_β (at.%)	C_α (at.%)	C_m (at.%)	D_0 (m ² /s)	Q_D (kJ/mol)
370	0.25	0.33	0.00857	0	4.44×10^{-5}	133.9
540	0.25	0.33	0.0216	0	4.44×10^{-5}	133.9

$$V_e = N \cdot \frac{4\pi}{3} \cdot (R_0^3 - R^3) \tag{22}$$

where N represents the number of secondary phase particles in a studied system. Substituting Eq. (21) into Eq. (22) and after an arrangement, it is obtained,

$$V_e = \frac{4\pi N}{3} \cdot \left\{ \begin{aligned} &3R_0 \cdot \left(\sqrt{\frac{k}{\pi}} \cdot (R_1 - \sqrt{kDt}) + \sqrt{R_1^2 - kDt} \right) \\ &\cdot \left(\frac{\sqrt{kDt}}{R_1 + \sqrt{R_1^2 - kDt}} + \sqrt{\frac{k}{\pi}} \right) \cdot (kDt)^{\frac{1}{2}} \\ &+ \left(\frac{\sqrt{kDt}}{R_1 + \sqrt{R_1^2 - kDt}} + \sqrt{\frac{k}{\pi}} \right)^3 \cdot (kDt)^{\frac{3}{2}} \end{aligned} \right\} \tag{23}$$

Modification by considering the interactions of multi-particle dissolution

Following the above analysis, a JMA-like equation can be deduced for dissolution in multi-particle dissolution. Substituting the initial volume, $V_0 = N4\pi R_0^3/3$ and the extended transformed volume (Eq. 22), the extended transformed fraction, x_e , can be rewritten as,

$$x_e = \frac{1}{R_0^3} \cdot (R_0^3 - R^3) \tag{24}$$

It is known that at the beginning of dissolution, the radius of the secondary phase equals to the initial radius ($R = R_0$), whereas, the radius decrease to zero ($R = 0$) once the dissolution process is completed. So the value of x_e changes from zero to unity during dissolution, i.e.,

$$0 \leq x_e \leq 1 \tag{25}$$

It is known that x_e is deduced by assuming that no interference occurs among adjacent particles during dissolution. In order to obtain the real transformed fraction, interactions in multi-particle system must be considered. If the classical JMA equation (Eq. 3) is applied to deal with such problem, the transformation degree (transformed fraction), f_t , lies then in the following range,

$$0 \leq f_t \leq 1 - e^{-1} \tag{26}$$

This implies that the classical JMA equation cannot describe the entire dissolution process; a modification of the classic JMA model is thus necessary.

Departing from the real essence of the extended transformed volume without considering the interferences among adjacent particles, the extended transformed volume upon dissolution cannot exceed the volume of the initial secondary phase. In order to perform the current modeling, it is assumed that the classic JMA theory hold valid during the entire transformation process, i.e., the JMA prediction is expanded to the real transformation process. On this basis, a modified transformed fraction, f_{tm} , and a correspondingly modified transformed time, t_m , are introduced; every modified transformed fraction unit, Δf_{tm} , equals to the proportional expansion of Δf_t , due to the classical JMA kinetics, and every modified transformed time unit, Δt_m , equals to the proportional expansion of Δt due to JMA. The proportional factor can be regarded approximately as a constant, m , for the entire transformation. Then, the following equations can be obtained,

$$\begin{cases} \int_0^{f_m} df_{tm} = \int_0^{f_t} mdf_t \\ \int_0^{t_m} dt_m = \int_0^t mdt \end{cases} \tag{27}$$

Accordingly, the modified transformed fraction, f_{tm} , and time, t_m , can be expressed as,

$$\begin{cases} f_{tm} = mf_t = m \cdot (1 - \exp(-x_e)) \\ t_m = m \cdot t \end{cases} \tag{28}$$

Clearly, f_{tm} changes from zero to the unity during the entire dissolution process. The proportional factor, m , can be obtained from the complete integral, $\int_0^1 df_{tm} = \int_0^{1-e^{-1}} mdf_t$ which gives,

$$m = \frac{1}{1 - e^{-1}} = \frac{e}{e - 1} \tag{29}$$

Combining Eqs. (2) and (28) gives,

$$f_{tm} = \frac{f - f_0}{f_{eq} - f_0} = m \cdot (1 - \exp(-x_e)) \tag{30}$$

Then the volume fraction of the secondary phase, f , can be obtained as,

$$f = (m \cdot f_{eq} + (1 - m) \cdot f_0) + [f_0 - (m \cdot f_{eq} + (1 - m) \cdot f_0)] \exp(-x_e) \tag{31}$$

where x_e is obtained by combining Eqs. (22), (24), and (28) as,

$$x_e = \frac{1}{R_0^3} \cdot \left\{ \begin{aligned} &3R_0 \cdot \left(\sqrt{\frac{k}{\pi}} \cdot \left(R_1 - \sqrt{\frac{kDt_m}{m}} \right) + \sqrt{R_1^2 - \frac{kDt_m}{m}} \right) \\ &\cdot \left(\frac{\sqrt{kDt_m}}{\sqrt{m} \cdot R_1 + \sqrt{mR_1^2 - kDt_m}} + \sqrt{\frac{k}{\pi}} \right) \cdot \left(\frac{kDt_m}{m} \right)^{\frac{1}{2}} \\ &+ \left(\frac{\sqrt{kDt_m}}{\sqrt{m} \cdot R_1 + \sqrt{mR_1^2 - kDt_m}} + \sqrt{\frac{k}{\pi}} \right)^3 \cdot \left(\frac{kDt_m}{m} \right)^{\frac{3}{2}} \end{aligned} \right\} \quad (32)$$

Model description

In the current model, the interaction of the diffusion fields is described by modification of the JMA theory, and a mathematical expression for the extended transformed fraction, x_e , (Eq. 32) upon dissolution is developed following the classic diffusion theory. Applying the current model, a physically realistic description for dissolution in multi-particle system becomes possible.

The current model is correlated with several key parameters, such as: f_0 , f_{eq} , R_1 , R_0 , and k . Values of f_0 and f_{eq} are related to the initial and final thermodynamic states, respectively. Generally, dissolution occurs in the single-phase region of the phase diagram, which means the value of f_{eq} equals to zero in most cases. As expressed in Eq. (20), the value of R_1 depends on R_0 (the initial radius of the secondary phase particle) and k (as function of the pertinent concentrations, C_β , C_α , and C_m , (Eq. 8), which depend on the thermodynamic state of the dissolution system). Given f_0 , f_{eq} , R_0 , C_β , C_α , and C_m , the dissolution process can thus be described using the current model.

When compared with the numerical results performed by Wang et al. [37] using PFM, the evolution of the secondary phase volume fraction with time is calculated using Eq. (31) (Fig. 3). Meanwhile, the evolution due to the classic analytical model (Eq. 7) and the semiempirical model (Eq. 4) are also shown. Upon dissolution, interferences between particles will slow down the transformation rate, implying that the classic analytical model for single-particle system developed by Whelan [21] is invalid. Although the semiempirical model can describe well the dissolution process, such model is not derived from the diffusion kinetics during dissolution, i.e., it cannot reflect physically the diffusion-controlled transformation mechanism. The current analytical solution derived from the diffusion-controlled transformation theory resembles closely the real process. Values of the parameters used are chosen from dissolution in Ni–Al alloy [37].

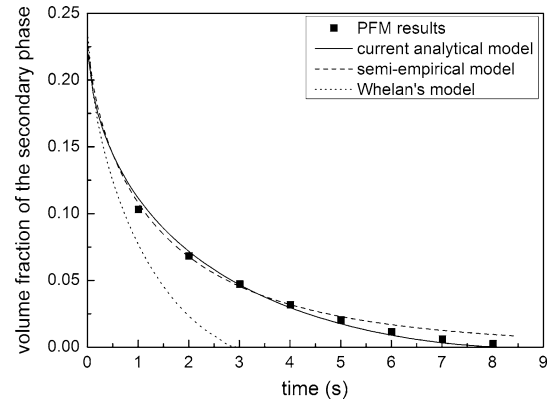


Fig. 3 Comparisons between the PFM result developed by Wang et al. [37] and the prediction due to the current model (Eq. 31), as well as the classic dissolution (Eq. 7) and semiempirical models (Eq. 4), for the volume fraction of the secondary phase upon dissolution at 1444 K in Ni–Al alloy [37]

Peculiarity of current model: time-dependent transformation coefficients

Generally, according to semiempirical models [37, 41–44], the volume fraction of the secondary phase upon isothermal dissolution can be expressed as Eq. (4), where the parameter, K follows an Arrhenius relation, $K_0 \exp(-Q/R_g T)$ with K_0 as the rate constant, Q the activation energy for dissolution, and R_g the gas constant. Thus, Eq. (4) can be rewritten as,

$$f = f_{eq} + (f_0 - f_{eq}) \exp\left(-K_0^n \exp\left(-\frac{nQ}{R_g T}\right) \cdot t^n\right) \quad (33)$$

Clearly, Eq. (33) has a similar structure as the current model (Eq. 31) by modifying only the parameter ‘ f_{eq} ’ into the term ‘ $m \cdot f_{eq} + (1 - m) \cdot f_0$ ’. In previous semiempirical models, values of n , K in Eq. (4) are determined solely by fitting to the experimental results as constant, whereas, time-dependent parameters, n , K_0 can be obtained in the current model, using a mathematical treatment analogous to that performed in Ref. [47, 48].

Extended fraction treatment due to Ref. [47]

The overall extended transformed fraction x_e , due to Eq. (32) is composed of two parts: x_{e1} and x_{e2} ,

$$\left\{ \begin{aligned} &x_{e1} = \frac{1}{R_0^3} \cdot 3R_0 \cdot \left(\sqrt{\frac{k}{\pi}} \cdot \left(R_1 - \sqrt{\frac{kDt_m}{m}} \right) + \sqrt{R_1^2 - \frac{kDt_m}{m}} \right) \\ &\cdot \left(\frac{\sqrt{kDt_m}}{\sqrt{m} \cdot R_1 + \sqrt{mR_1^2 - kDt_m}} + \sqrt{\frac{k}{\pi}} \right) \cdot \left(\frac{kDt_m}{m} \right)^{\frac{1}{2}} \\ &x_{e2} = \frac{1}{R_0^3} \cdot \left(\frac{\sqrt{kDt_m}}{\sqrt{m} \cdot R_1 + \sqrt{mR_1^2 - kDt_m}} + \sqrt{\frac{k}{\pi}} \right)^3 \cdot \left(\frac{kDt_m}{m} \right)^{\frac{3}{2}} \end{aligned} \right. \quad (34)$$

The ratio of x_{e1} and x_{e2} is given by,

$$\frac{x_{e2}}{x_{e1}} = \frac{\left(\frac{\sqrt{kDt_m}}{\sqrt{m} \cdot R_1 + \sqrt{mR_1^2 - kDt_m}} + \sqrt{\frac{k}{\pi}}\right)^2 \cdot \frac{kD}{m} \cdot t_m}{3R_0 \cdot \left(\sqrt{\frac{k}{\pi}} \cdot \left(R_1 - \sqrt{\frac{kDt_m}{m}}\right) + \sqrt{R_1^2 - \frac{kDt_m}{m}}\right)} = \frac{a_2}{a_1} \tag{35}$$

Now, a mathematical treatment analogous to that in Ref. [47] is performed to obtain explicit, analytical expressions for the transformed exponent n and the rate constant K_0 . And Eq. (32) can be rewritten as (see “Appendix”),

$$x_e = \left\{ \begin{array}{l} \frac{1}{R_0^3} \cdot \left(\frac{kDt_m}{m}\right)^{\frac{1}{2} + \frac{1}{1 + \left(\frac{a_2}{a_1}\right)^{-1}}} \cdot \left(\frac{\sqrt{kDt_m}}{\sqrt{m} \cdot R_1 + \sqrt{mR_1^2 - kDt_m}} + \sqrt{\frac{k}{\pi}}\right)^{1 + \frac{2}{1 + \left(\frac{a_2}{a_1}\right)^{-1}}} \cdot \left(1 + \left(\frac{a_2}{a_1}\right)^{-1}\right)^{\frac{1}{1 + \left(\frac{a_2}{a_1}\right)^{-1}}} \\ \left[3R_0 \cdot \left(\sqrt{\frac{k}{\pi}} \cdot \left(R_1 - \sqrt{\frac{kDt_m}{m}}\right) + \sqrt{R_1^2 - \frac{kDt_m}{m}}\right) \cdot \left(1 + \frac{a_2}{a_1}\right)\right]^{\frac{1}{1 + \frac{a_2}{a_1}}} \end{array} \right\} \tag{36}$$

Since, the diffusion coefficient D follows as an Arrhenius structure,

$$D = D_0 \exp\left(-\frac{Q_D}{R_g T}\right) \tag{37}$$

with D_0 as the preexponential factor for diffusion and Q_D the activation energy for diffusion, Eq. (36) can then be rewritten as,

where a_2/a_1 depends on the transformation time (Eq. 35). This result can be compared with the correspondingly rewritten Eq. (33),

$$\ln(x_e) = \ln K_0^n - \frac{nQ}{R_g T} + n \ln t \tag{39}$$

By comparing Eqs. (38) and (39), the time-dependent expressions for n and K_0 can be obtained,

$$n = \frac{1}{2} + \frac{1}{1 + \left(\frac{a_2}{a_1}\right)^{-1}} \tag{40a}$$

$$K_0^n = \left\{ \begin{array}{l} \frac{1}{R_0^3} \cdot \left(\frac{kD_0}{m}\right)^{\frac{1}{2} + \frac{1}{1 + \left(\frac{a_2}{a_1}\right)^{-1}}} \cdot \left(\frac{\sqrt{kDt_m}}{\sqrt{m} \cdot R_1 + \sqrt{mR_1^2 - kDt_m}} + \sqrt{\frac{k}{\pi}}\right)^{1 + \frac{2}{1 + \left(\frac{a_2}{a_1}\right)^{-1}}} \cdot \left(1 + \left(\frac{a_2}{a_1}\right)^{-1}\right)^{\frac{1}{1 + \left(\frac{a_2}{a_1}\right)^{-1}}} \\ \left[3R_0 \cdot \left(\sqrt{\frac{k}{\pi}} \cdot \left(R_1 - \sqrt{\frac{kDt_m}{m}}\right) + \sqrt{R_1^2 - \frac{kDt_m}{m}}\right) \cdot \left(1 + \frac{a_2}{a_1}\right)\right]^{\frac{1}{1 + \frac{a_2}{a_1}}} \end{array} \right\} \tag{40b}$$

The effective activation energy for dissolution, Q , equals to the activation energy for diffusion, Q_D ; this confirms the prevalence of long-range diffusion control mechanism upon dissolution.

$$Q = Q_D \tag{40c}$$

Therefore, the volume fraction of the secondary phase upon isothermal dissolution can be represented by,

$$\ln(x_e) = \left\{ \begin{array}{l} \ln \left\{ \frac{1}{R_0^3} \cdot \left(\frac{kD_0}{m}\right)^{\frac{1}{2} + \frac{1}{1 + \left(\frac{a_2}{a_1}\right)^{-1}}} \cdot \left(\frac{\sqrt{kDt_m}}{\sqrt{m} \cdot R_1 + \sqrt{mR_1^2 - kDt_m}} + \sqrt{\frac{k}{\pi}}\right)^{1 + \frac{2}{1 + \left(\frac{a_2}{a_1}\right)^{-1}}} \cdot \left(1 + \left(\frac{a_2}{a_1}\right)^{-1}\right)^{\frac{1}{1 + \left(\frac{a_2}{a_1}\right)^{-1}}} \right. \\ \left. \left[3R_0 \cdot \left(\sqrt{\frac{k}{\pi}} \cdot \left(R_1 - \sqrt{\frac{kDt_m}{m}}\right) + \sqrt{R_1^2 - \frac{kDt_m}{m}}\right) \cdot \left(1 + \frac{a_2}{a_1}\right)\right]^{\frac{1}{1 + \frac{a_2}{a_1}}} \right\} \\ - \frac{\left(\frac{1}{2} + \frac{1}{1 + \left(\frac{a_2}{a_1}\right)^{-1}}\right) Q_D}{R_g T} + \left(\frac{1}{2} + \frac{1}{1 + \left(\frac{a_2}{a_1}\right)^{-1}}\right) \ln t_m \end{array} \right\} \tag{38}$$

$$f = (m \cdot f_{\text{eq}} + (1 - m) \cdot f_0) + [f_0 - (m \cdot f_{\text{eq}} + (1 - m) \cdot f_0)] \times \exp\left(-K_0(t)^{n(t)} \exp\left(-\frac{n(t)Q}{R_g T}\right) \cdot t^{n(t)}\right) \quad (41)$$

where the kinetic parameters, n and K_0 are time dependent.

Real expressions for time-dependent parameters

Generally, the value of the transformed exponent, n , is related to the transforming manner [43, 46]. For instance, when $n = 0.5$, plate-like particles show 1D diffusion-controlled growth in the direction of the height, while when $n = 1.5$, spherical particles show 3D diffusion-controlled growth. Following the above analysis for 3D diffusion-controlled dissolution, however, n is no longer a constant but a time-dependent coefficient, mainly due to the different transformed mechanisms between growth and dissolution. Upon growth, simple parabolic growth law prevails, whereas, upon dissolution, two different parts contribute to the entire transformation: x_{e1} and x_{e2} . Evolution of n with t during γ' dissolution in a Ni–Al alloy is described in Fig. 4, where, the value of n approaches to 0.5 if x_{e1} plays the dominant role, i.e., the ratio, a_2/a_1 approaches to zero, whereas, the value of n approaches to 1.5 if x_{e2} takes over the transformation.

When compared to the diffusion-controlled growth process, the value of n for 3D diffusion-controlled dissolution does not equal to a constant, 1.5, but changes from 0.5 to 1.5, indicating a continuous change of the prevailing role from x_{e1} to x_{e2} during transformation. Moreover, the value of n increases slowly from 0.5 intensely to 1.5, as the dissolution is about to be completed. Such phenomenon indicates that the x_{e1} part plays a more important role than the x_{e2} part, especially at the early stage. This is consistent with the values of n fitted by the semiempirical models during 3D dissolution. For instance, Wang et al. [37]

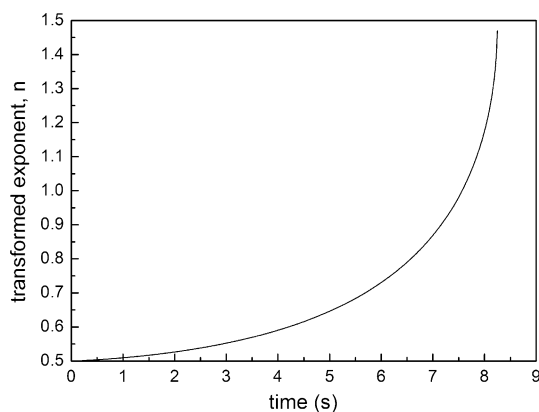


Fig. 4 Upon γ' dissolution at 1444 K in Ni–Al alloy, the transformed exponent, n , is described as a function of time. The calculation is performed by Eq. (40a)

concluded the value of n as equal to 0.688 for γ' dissolution in Ni–Al alloy, while Fukumoto et al. [43] concluded the value of n as ranged from 0.49 to 0.73 for δ -ferrite dissolution in an austenitic stainless steel. The fitted results lie in the range predicted by the current model.

Model application

In this section, the current model is adopted to describe some experimental data from Hewitt and Butler [15] for isothermal dissolution of θ' in Al–3.0wt%–Cu alloy, and from Tundal and Ryum [16] for isothermal dissolution of silicon particles in Al–0.8wt%–Si alloy. Moreover, evolution of the transformed exponent, n , for the secondary phase with various initial radii, R_0 and at different transformation temperatures during dissolution, is studied.

Isothermal dissolution of θ' in an Al–3.0wt%–Cu alloy

Hewitt and Butler [15] investigated the isothermal dissolution of θ' in Al–3.0wt%–Cu alloy. The alloy was solution heat treated at 550 °C for 30 min, then quenched into water. After that, samples were aged at 285 °C for 22 h to precipitate the secondary phase, θ' , in the microstructure. Then, a series of up-quenching experiments at 370 °C were performed. The corresponding dissolution process of θ' in the microstructure was observed in an EM7 high voltage electron microscope. A timed sequence of micrographs was obtained using a data acquisition system. Applying a stereometric analysis software, initial radii of over 20 individual particles, and the area of θ' at each time step were determined [15]. The mean size and standard deviation of the size distribution were calculated, as listed in Table 2. The initial sizes of θ' particles were found to be not much different from the average size, so that the corresponding initial radii of particles were regarded approximately as identical. Dissolution data were digitized using “GetData” software. The volume fraction of the secondary phase is found as a function of time, as shown in Fig. 5a, where the current model (Eq. 31) is applied to describe the dissolution process as well. Meanwhile, in order to understand the transformation process better, evolution of the transformed fraction, i.e., the transformation degree during dissolution

Table 2 The mean size and standard deviation of the size distribution for dissolution of θ' in an Al–3.0wt%–Cu alloy and dissolution of silicon particles in an Al–0.8wt%–Si alloy

References	Mean size (μm)	Standard deviation
[15]	0.25	0.028
[16]	1.89	0.17

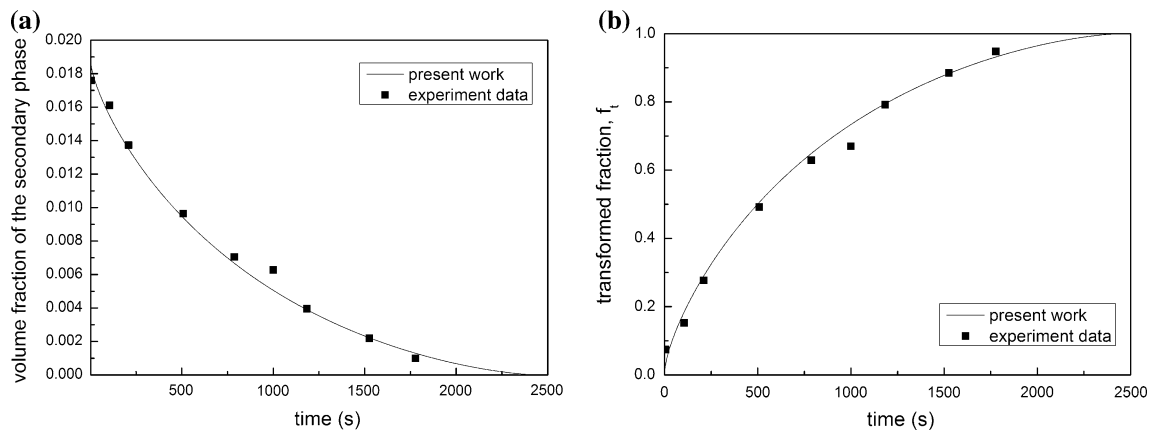


Fig. 5 Upon isothermal dissolution of Al–3.0wt%–Cu alloy at 370 °C, **a** evolution of the volume fraction of the secondary phase with time; **b** evolution of the transformed fraction (transformation

degree), f_t , with time. Experimental data are obtained from Ref. [15, 49] and the theoretical prediction is performed by the current work

Table 3 Parameters used for the current model prediction for dissolution of θ' in an Al–3.0wt%–Cu

References	T (°C)	f_0	f_{eq}	R_0 (μm)	C_β (at.%)	C_x (at.%)	C_m (at.%)	D_0 (m^2/s)	Q_D (kJ/mol)
[15, 49]	370	0.019	0	0.25	0.33	0.00857	0	4.44×10^{-5}	133.9

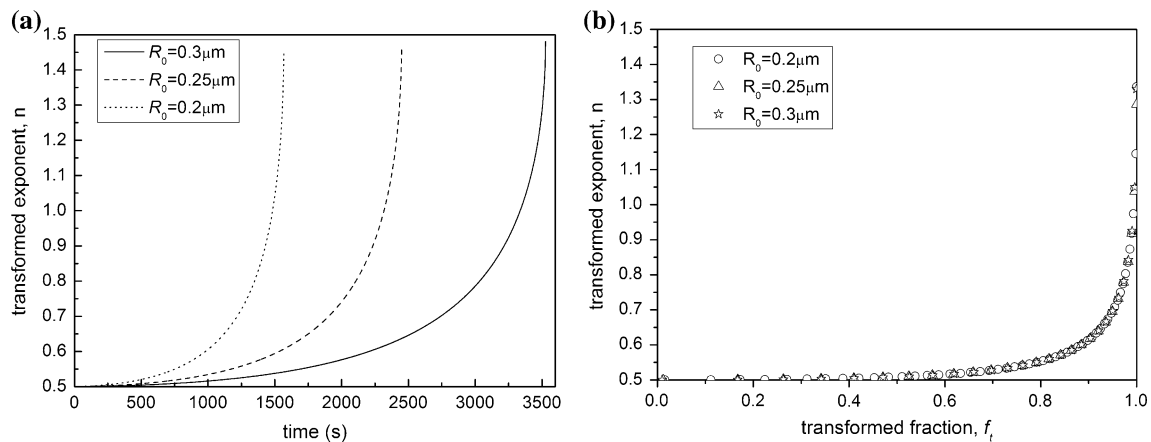


Fig. 6 Upon dissolution of θ' at three different initial radii, 0.2, 0.25, and 0.3 μm , in the Al–3.0wt%–Cu alloy at 370 °C, evolutions of the transformed exponent, n , with **a** time and **b** transformed fraction are described, respectively

is performed, as shown in Fig. 5b. Corresponding parameters used for modeling θ' dissolution in Al–3.0wt%–Cu alloy are listed in Table 3. As mentioned above (Eq. 37), the diffusion coefficient, D , can be calculated by an Arrhenius equation, and D_0 , Q_D for copper diffusing in aluminum can be found in Ref. [49]. Values of parameters, f_0 , f_{eq} , R_0 , C_β , C_x , and C_m , are from Ref. [15]. On this basis, good agreement between the current model prediction and the experimental data is obtained.

As shown in Sect. “Peculiarity of current model: time-dependent transformation coefficients”, the transformed exponent, n , is not a constant, but increases with the transformation time during 3D diffusion-controlled dissolution.

Here, in order to study the effect of the initial state of dissolving particles for the transformation process, three various initial radii, 0.2, 0.25, and 0.3 μm , are given. Then, as shown in Fig. 6a, the evolution of n with t is obtained, where the initial radius, R_0 , is of great effect on the transformed exponent, n . Larger R_0 corresponds with more dissolution time, so that the value of n increases more slowly to 1.5. However, as shown in Fig. 6b, the evolution of n with f_t holds the same for different R_0 , which means the value of n , remains unchanged at a given transformed fraction for various R_0 during the entire transformation process. This also indicates that the x_{e1} part in Eq. (34) play a more important role than the x_{e2} part during dissolution.

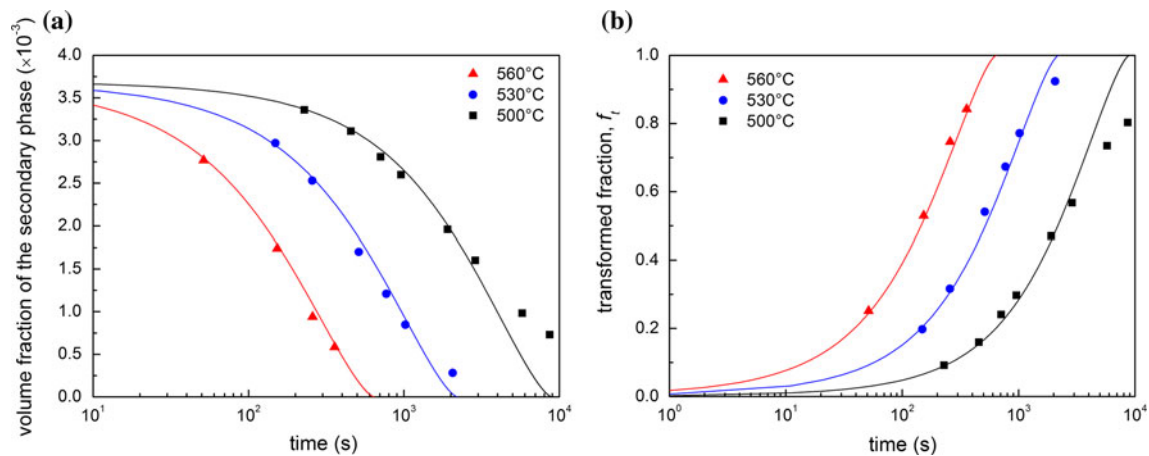


Fig. 7 Evolutions of **a** the volume fraction of silicon particles and **b** transformed fraction with time during isothermal dissolution in an Al-0.8wt%-Si alloy at 500, 530, and 560 °C, respectively.

Experimental data are from Ref. [16] and the theoretical prediction is performed by the current work

Table 4 Parameters used for the current model prediction for dissolution of silicon particles in an Al-0.8wt%-Si alloy

References	T (°C)	f_0	f_{eq}	R_0 (μm)	C_β (at.%)	C_x (at.%)	C_m (at.%)	D_0 (m^2/s)	Q_D (kJ/mol)
[16]	500	0.0037	0	1.89	0.8289	0.0079	0.0046	2.02×10^{-4}	139
	530	0.0037	0	1.89	0.8289	0.0104	0.0046		
	560	0.0037	0	1.89	0.8289	0.0136	0.0046		

Isothermal dissolution of silicon particles in Al-0.8wt%-Si alloy

With reference to [16], Al-0.8wt %-Si alloy was produced in laboratory scale by directional solidification. Then, the casting was homogenized for 48 h at 580 °C. After that, the alloy was heat treated at 490 °C for 24 h, 70 % cold rolled, held for 4 h at 490 °C, cooled at 1 °C/h to 450 °C and heat treated for another 48 h to obtain spherical particles. The dissolution reaction was studied by up-quenching the specimens in a salt bath to various temperatures above the solvus temperature. Then, the specimens were quenched in cold water. Using a semiautomatic image analyzer, 3541 particles in an area of 12 mm² were measured, and the sizes of particles after each heat treatment were determined. The mean size and standard deviation of the size distribution were calculated, as listed in Table 2. The initial sizes of silicon particles were found to be not much different from the average size, so that the corresponding initial radii of particles were regarded approximately as identical. The area fraction of precipitates found using image analysis was then plotted with time.

As mentioned above, all specimens have the same initial thermodynamic states, i.e., the same initial volume fraction, f_0 , radius, R_0 , solute concentration in the secondary phase, C_β , and matrix, C_m , while different heat treatment temperatures

result in different thermodynamic equilibrium concentration in the matrix, C_x , and corresponding diffusion coefficient. So the heat treatment temperature will influence the dissolution process. Tundal and Ryum [16] observed spherical silicon particles dissolving in Al-0.8wt%-Si alloy at 500, 530, and 560 °C, respectively. The volume fraction of the secondary phase is found as a function of time, as shown in Fig. 7a, where the current model (Eq. 31) is applied to describe the dissolution process as well. Meanwhile, in order to understand the transformation process better, evolution of the transformed fraction, i.e., the transformation degree during dissolution is performed, as shown in Fig. 7b. Good agreement is obtained for all three temperatures. The relevant parameters for calculation are from Ref. [16] (see Table 4).

Meanwhile, at different heat treatment temperatures, the evolution of transformed exponent, n , with time is performed, as shown in Fig. 8a, where the transformation temperature is of great effect on the transformed exponent, n . It can be seen lower transformation temperature leads to more transformation time, so that the value of n increases more slowly to 1.5. However, as shown in Fig. 8b, the evolution of n with f_t holds the same for different transformation temperatures, i.e., the value of n , which increases slowly from 0.5 and intensely to 1.5, remain unchanged at a given transformed fraction for different heat treatment temperatures during the entire transformation process. This

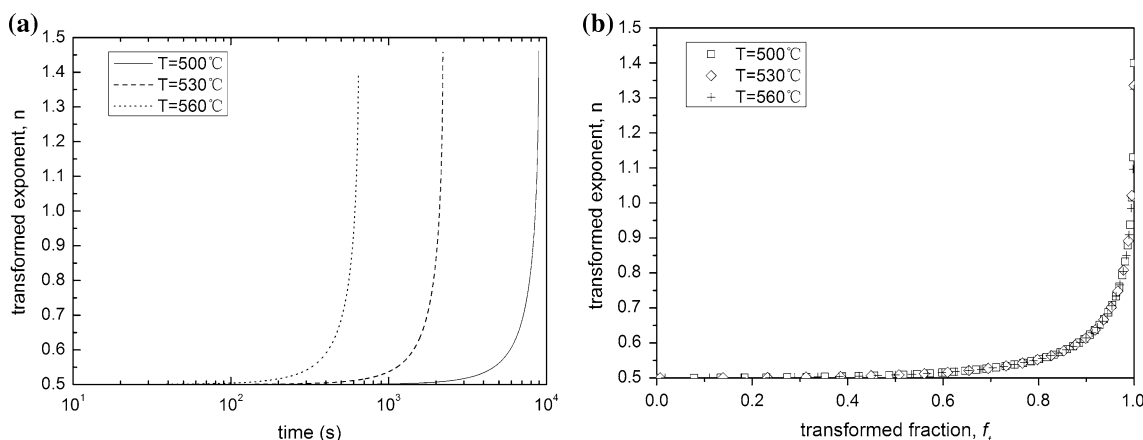


Fig. 8 Upon dissolution of silicon particles in an Al–0.8wt%–Si alloy at 500, 530, and 560 °C, respectively, the exponential factor, n , as a function of **a** time and **b** transformed fraction

also confirms that the x_{e1} part in Eq. (34) play a more important role than the x_{e2} part during dissolution.

When compared to the classical JMA kinetics, the current f_t-t curve follows a parabolic-like shape in 3D dissolution instead of the typical “S” shape in the classical JMA theory, the variation of n with f_t during the transformation is independent of the temperature, and the validity for application of the classical JMA kinetics into the dissolution kinetics needs more evidences. This is out of the main focus of the current work and will be studied in the future work.

Conclusion

Based on the JMA theory and the classical dissolution model for single-particle system, an analytical model for the secondary phase dissolution in multi-particle system has been developed. The interactions of solute diffusion fields in front of the secondary phase/matrix interface are considered in the current model. Numerical calculations have shown that the current model can give a clear and concise relationship between the secondary phase volume fraction and the time for isothermal dissolution. Compared with the semiempirical dissolution models, the current model follows an analogous form, but with time-dependent kinetic parameters. Most importantly, the current model is derived from the diffusion-controlled transformation theory, while the modeling quality is guaranteed by the physically realistic model parameters. The isothermal θ' dissolution in Al–3.0wt%–Cu alloy and silicon dissolution in Al–0.8wt%–Si alloy have been predicted using the current model; good agreement with the real process is achieved.

Acknowledgements The authors are grateful to the Natural Science Foundation of China (Nos. 51134011, 51101122, and 51071127), the National Basic Research Program of China (973 Program, No.

2011CB610403), China National Funds for Distinguished Young Scientists (No. 51125002), the Fundamental Research Fund (Nos. JC20120223), and the 111 Project (No. B08040) of Northwestern Polytechnical University.

Appendix

Analogous to a mathematical treatment in Ref. [47], the extended transformed fraction is reformulated proceeding as follows.

For the two parts x_{e1} and x_{e2} in Eq. (34), two corresponding parameters b_1 and b_2 can be chosen in such a way that x_e is due to only the first part,

$$x_{e1'} = \frac{b_1}{R_0^3} \cdot 3R_0 \cdot \left(\sqrt{\frac{k}{\pi}} \cdot \left(R_1 - \sqrt{\frac{kDt_m}{m}} \right) + \sqrt{R_1^2 - \frac{kDt_m}{m}} \right) \cdot \left(\frac{\sqrt{kDt_m}}{\sqrt{m} \cdot R_1 + \sqrt{mR_1^2 - kDt_m}} + \sqrt{\frac{k}{\pi}} \right) \cdot \left(\frac{kDt_m}{m} \right)^{\frac{1}{2}} \tag{A.1}$$

Or that x_e is due to only the second part,

$$x_{e2'} = \frac{b_2}{R_0^3} \cdot \left(\frac{\sqrt{kDt_m}}{\sqrt{m} \cdot R_1 + \sqrt{mR_1^2 - kDt_m}} + \sqrt{\frac{k}{\pi}} \right)^3 \cdot \left(\frac{kDt_m}{m} \right)^{\frac{3}{2}} \tag{A.2}$$

With $x_{e1'} = x_{e2'} = x_e$. Then, the total extended transformed fraction can be written as,

$$x_e = \frac{1}{a_1 + a_2} (a_1 \cdot x_{e1'} + a_2 \cdot x_{e2'}) \tag{A.3}$$

And

$$\begin{cases} b_1 = 1 + \frac{a_2}{a_1} \\ b_2 = 1 + \left(\frac{a_2}{a_1} \right)^{-1} \end{cases} \tag{A.4}$$

During dissolution, it can be seen that both x_{e1} and x_{e2} are positive and smaller than x_e . Always two integers, a_1 and a_2 , can be found to satisfy Eq. (35). Moreover, for integers, a_1 and a_2 , it holds that $a_1 x_{e1'} = \sum_{i=1}^{a_1} x_{e1}(i)$ if $x_{e1}(1) = x_{e1}(2) = \dots = x_{e1}(a_1) = x_{e1}'$; and $a_2 x_{e2'} = \sum_{i=1}^{a_2} x_{e2}(i)$ if $x_{e2}(1) = x_{e2}(2) = \dots = x_{e2}(a_2) = x_{e2}'$. Then, taking both $x_{e1}(i)$ and $x_{e2}(i)$ equal to x_e , Eq. (A.3) can be rewritten as,

$$x_e = \frac{1}{a_1 + a_2} \left(\sum_{i=1}^{a_1} x_{e1}(i) + \sum_{i=1}^{a_2} x_{e2}(i) \right) \quad (\text{A.5})$$

Note that all fraction terms in Eq. (A.5) are equal. Substituting all $x_{e1}(i)$ and $x_{e2}(i)$ combined with Eqs. (A.1), (A.2) and (A.4), Eq. (A.5) becomes,

$$x_e = \left\{ \begin{array}{l} \frac{1}{R_0^3} \cdot \left(\frac{kDt_m}{m} \right)^{\frac{1}{2} + \frac{1}{1 + \left(\frac{a_2}{a_1}\right)^{-1}}} \\ \cdot \left(\frac{\sqrt{kDt_m}}{\sqrt{m} \cdot R_1 + \sqrt{mR_1^2 - kDt_m}} + \sqrt{\frac{k}{\pi}} \right)^{1 + \frac{2}{1 + \left(\frac{a_2}{a_1}\right)^{-1}}} \\ \cdot \left(1 + \left(\frac{a_2}{a_1} \right)^{-1} \right)^{\frac{1}{1 + \left(\frac{a_2}{a_1}\right)^{-1}}} \\ \left[3R_0 \cdot \left(\sqrt{\frac{k}{\pi}} \cdot \left(R_1 - \sqrt{\frac{kDt_m}{m}} \right) + \sqrt{R_1^2 - \frac{kDt_m}{m}} \right) \right. \\ \left. \cdot \left(1 + \frac{a_2}{a_1} \right) \right]^{\frac{1}{1 + \frac{a_2}{a_1}}} \end{array} \right\} \quad (\text{A.6})$$

References

- Seiser B, Drautz R, Pettifor DG (2011) TCP phase predictions in Ni-based superalloys: structure maps revisited. *Acta Mater* 59:749–763
- Lo KH, Shek CH, Lai JKL (2009) Recent developments in stainless steels. *Mater Sci Eng R* 65:39–104
- Liu F, Cai Y, Guo XF, Yang GC (2000) Structure evolution in undercooled DD3 single crystal superalloy. *Mater Sci Eng A* 291:9–16
- Fan K, Liu F, Liu XN, Zhang YX, Yang GC, Zhou YH (2008) Modeling of isothermal solid-state precipitation using an analytical treatment of soft impingement. *Acta Mater* 56:4309–4318
- Clavaguera-Mora MT, Clavaguera N, Crespo D, Pradell T (2002) Crystallisation kinetics and microstructure development in metallic systems. *Prog Mater Sci* 47:559–619
- Crespo D, Pradell T, Clavaguera-Mora MT, Clavaguera N (1997) Microstructure evaluation of primary crystallization with diffusion-controlled grain growth. *Phys Rev B* 55:3435–3444
- Pradell T, Crespo D, Clavaguera N, Clavaguera-Mora MT (1998) Diffusion controlled grain growth in primary crystallization: Avrami exponents revisited. *J Phys* 10:3833–3844
- Tkatch VI, Rassolov SG, Moiseeva TN, Popov VV (2005) Analytical description of isothermal primary crystallization kinetics of glasses: Fe₈₅B₁₅ amorphous alloy. *J Non Cryst Solids* 351:1658–1664
- Chen YZ, Yang GC, Liu F, Liu N, Xie H, Zhou YH (2005) Microstructure evolution in undercooled Fe-7.5 at% Ni alloys. *J Cryst Growth* 282:490–497
- Liu N, Liu F, Yang GC, Chen YZ, Chen D, Yang CL, Zhou YH (2007) Grain refinement of undercooled single-phase Fe₇₀Co₃₀ alloys. *Phys B* 387:151–155
- Ge Yu, Lai YKL, Zhang W (1997) Kinetics of transformation with nucleation and growth mechanism: diffusion-controlled reactions. *J Appl Phys* 82:4270–4276
- Wang HF, Liu F, Zhang T, Yang GC, Zhou YH (2009) Kinetics of diffusion-controlled transformations: application of probability calculation. *Acta Mater* 57:3072–3083
- Roncery LM, Weber S, Theisen W (2011) Nucleation and precipitation kinetics of M₂₃C₆ and M₂N in an Fe–Mn–Cr–C–N austenitic matrix and their relationship with the sensitization phenomenon. *Acta Mater* 59:6275–6286
- Zheng Y, Zheng YF, Jiang F, Li L, Yang H, Liu YN (2008) Effect of ageing treatment on the transformation behaviour of Ti–50.9 at.% Ni alloy. *Acta Mater* 56:736–745
- Hewitt P, Butler EP (1986) Mechanisms and kinetics of θ' dissolution in Al-3% Cu. *Acta Metall* 34:1163–1172
- Tundal UH, Ryum N (1992) Dissolution of particles in binary alloys: Part II. Experimental investigation on an Al–Si alloy. *Metall Trans A* 23:445–449
- Katona GL, Erdélyi Z, Beke DL, Dietrich Ch, Weigl F, Boyen HG, Koslowski B, Ziemann P (2005) Experimental evidence for a nonparabolic nanoscale interface shift during the dissolution of Ni into bulk Au(111). *Phys Rev B* 11:115432-1–115432-5
- Milhet X, Arnoux M, Pelosin V, Colin J (2012) On the dissolution of the γ' phase at the dendritic scale in a rhenium-containing nickel-based single crystal superalloy after high temperature exposure. *Metall Mater Trans A* 44:2031–2040
- Thomas G, Whelan MJ (1961) Observations of precipitation in thin foils of aluminium +4 % copper alloy. *Phil Mag* 6:1103–1114
- Aaron HB (1968) On the kinetics of precipitate dissolution. *Metal Sci J* 2:192–193
- Whelan MJ (1969) On the kinetics of precipitate dissolution. *Metal Sci J* 3:95–97
- Aaron HB, Fainstein D, Kotler GR (1970) Diffusion-limited phase transformations: a comparison and critical evaluation of the mathematical approximations. *J Appl Phys* 41:4404–4410
- Nolfi FV Jr, Shewmon PG, Foster JS (1970) The dissolution kinetics of Fe₃C in ferrite—a theory of interface migration. *Metall Trans* 1:2291–2298
- Aaron HB, Kotler GR (1971) Second phase dissolution. *Metall Trans* 2:393–408
- Enomoto M, Nojiri N (1997) Influence of interfacial curvature on the growth and dissolution kinetics of a spherical precipitate. *Scripta Mater* 36:625–632
- Nojiri N, Enomoto M (1995) Diffusion-controlled dissolution of a spherical precipitate in an infinite binary alloy. *Scripta Metall Mater* 32:787–791
- Brown LC (1976) Diffusion controlled dissolution of planar, cylindrical, and spherical precipitates. *J Appl Phys* 47:449–458
- Tanzilli RA, Heckel RW (1968) Numerical solutions to the finite, diffusion-controlled, two phase, moving-interface problem (with planar, cylindrical, and spherical interfaces). *Trans AIME* 242:2313–2321
- Tanzilli RA, Heckel RW (1969) A normalized treatment of the solution of second phase particles. *Trans Met Soc AIME* 245:1363–1366
- Baty DL, Tanzilli RA, Heckel RW (1970) Solution kinetics of CuAl₂ in an Al–4Cu alloy. *Metall Trans* 1:1651–1656

31. Tundal UH, Ryum N (1992) Dissolution of particles in binary alloys: Part I. Computer simulations. *Metall Trans A* 23:433–444
32. Vermolen F, Vуйk K, van der Zwaag S (1998) A mathematical model for the dissolution kinetics of Mg₂Si-phases in Al–Mg–Si alloys during homogenisation under industrial conditions. *Mater Sci Eng A* 254:13–32
33. Chen LQ (2002) Phase-field models for microstructure evolution. *Annu Rev Mater Res* 32:113–140
34. Moelans N, Blanpain B, Wollants P (2008) An introduction to phase-field modeling of microstructure evolution. *Calphad* 32:268–294
35. Javierre E, Vuik C, Vermolen FJ, Segal A (2007) A level set method for three dimensional vector Stefan problems: dissolution of stoichiometric particles in multi-component alloys. *J Comput Phys* 224:222–240
36. Chen LQ, Wang Y (1996) The continuum field approach to modeling microstructural evolution. *JOM* 48:13–18
37. Wang G, Xu DS, Ma N, Zhou N, Payton EJ, Yang R (2009) Simulation study of effects of initial particle size distribution on dissolution. *Acta Mater* 57:316–325
38. Ghosh G (2001) Dissolution and interfacial reactions of thin-film Ti/Ni/Ag metallizations in solder joints. *Acta Mater* 49:2609–2624
39. Chen Q, Ma N, Wu K, Wang Y (2004) Quantitative phase field modeling of diffusion-controlled precipitate growth and dissolution in Ti–Al–V. *Scripta Mater* 50:471–476
40. Kovacevic I, Sarler B (2005) Solution of a phase-field model for dissolution of primary particles in binary aluminum alloys by an r-adaptive mesh-free method. *Mater Sci Eng A* 413–414:423–428
41. Cormier J, Milhet X, Mendez J (2007) Effect of very high temperature short exposures on the dissolution of the γ' phase in single crystal MC₂ superalloy. *J Mater Sci* 42:7780–7786. doi:10.1007/s10853-007-1645-3
42. Giraud R, Hervier Z, Cormier J, Saint-Martin G, Hamon F, Milhet X, Mendez J (2012) Strain effect on the γ' dissolution at high temperatures of a nickel-based single crystal superalloy. *Metall Mater Trans A* 44:131–146
43. Fukumoto S, Iwasaki Y, Motomura H, Fukuda Y (2012) Dissolution behavior of δ -ferrite in continuously cast slabs of SUS304 during heat treatment. *ISIJ Int* 52:74–79
44. Ferro P (2013) A dissolution kinetics model and its application to duplex stainless steels. *Acta Mater* 61:3141–3147
45. Mittemeijer EJ (1992) Review: analysis of the kinetics of phase transformations. *J Mater Sci* 27:3977–3987. doi:10.1007/BF01105093
46. Christian JW (2002) *The theory of transformations in melts and alloys*. Pergamon, Oxford
47. Liu F, Sommer F, Mittemeijer EJ (2004) An analytical model for isothermal and isochronal transformation kinetics. *J Mater Sci* 39:1621–1634. doi:10.1023/B:JMISC.0000016161.79365.69
48. Liu F, Yang C, Yang G, Zhou Y (2007) Additivity rule, isothermal and non-isothermal transformations on the basis of an analytical transformation model. *Acta Mater* 55:5255–5267
49. Zhang RJ, Jing T, Jie WQ, Liu BC (2006) Phase-field simulation of solidification in multicomponent alloys coupled with thermodynamic and diffusion mobility databases. *Acta Mater* 54:2235–2239